International Journal of Environmental Sciences
ISSN: 2229-7359
Vol. 12 No. 1s, 2026
https://theaspd.com/index.php

Sustainable Agro-Economic Development in Hyper-Arid Zones: Local Biochar Amendments as a Resource-Saving Strategy for Desert Wheat Cultivation

Omar Mostefaoui[1], Abdelmalek Zaater[2,3], Khaled Laîche[4]

[1]Faculty of Economic, commercial and Management sciences, University of El-Oued, El-Oued 39000, Algeria.
*Corresponding Author Email: mostefaoui-omar@univ-eloued.dz ORCID: 0000-0003-2896-0647
[2]Faculty of natural sciences and life, University of El-Oued, El-Oued 39000, Algeria
[3]Laboratory of Biodiversity and application of biotechnology in the agricultural field, Faculty of natural sciences and life, University of El Oued, El-Oued 39000, Algeria, Email: abdelmalek-zaater@univ-eloued.dz ORCID: 0000-0002-1472-9954
[4] Faculty of natural sciences and life, University of El-Oued, El-Oued 39000, Algeria, Email:laiche-khaled@univ-eloued.dz ORCID: 0000-0002-0295-6632

Received: 15/2/2026 **Accepted**: 22/04/2026 **Published**: 30/05/2026

Abstract

An experimental study was conducted in the hyper-arid environment of El Oued city-Algeria, to evaluate the impact of various soil amendments (T0, T7) on soil moisture hydrodynamics, seed germination, and final crop productivity. The local core daytime microclimatic conditions during February featured solar radiation peaking at approximately 700 W/m^2 at solar noon, with ambient air temperatures fluctuating between a morning minimum of 10.5°C and a mid-afternoon maximum of 20.5°C. Hydrodynamic monitoring over a full 16-day cycle revealed that unamended native Saharan sand (T0) exhibited severe water-holding limitations, with volumetric moisture content collapsing precipitously from 80% to a critical minimum of 0% by Day 5. Conversely, carbonaceous biochar amendments (T3, T4) successfully established an internal capillary reservoir, sustaining elevated moisture configurations (=70%) through the initial desiccation phase. Biological monitoring revealed an intriguing agronomic paradox regarding early seedling establishment: the loose, macro-porous structure of raw control sand (T0) offered minimal physical impedance, securing the highest initial seed germination rate at 93%, followed closely by biochar blends T4 (90%) and T3 (89%), while treatment T2 heavily suppressed initial emergence to an absolute minimum of 50%. However, final structural harvest data collected at maturity demonstrated a complete inversion of these early vegetative trends. The unamended control sand (T0) produced heavily stunted ears capping at a meager 12.0 cm due to chronic late-stage moisture deficits and thermal stress. In contrast, the optimized structural composite amendment T6 yielded the absolute maximum final agronomic performance, achieving an optimal average ear length of 18.0 cm, followed closely by T5 (17.0 cm) and the biochar cohorts (16.0 cm). These findings explicitly demonstrate that while raw desert sand facilitates rapid initial sprouting, its severe evaporative desiccation neutralizes early growth advantages. Ultimately, the long-term hydro-thermal buffering and structural matrix modifications provided by advanced amendments–specifically T6, T5, and biochar configurations are the decisive factors required to secure optimal reproductive development and sustainable crop yields in hyper-arid agricultural zones.

Keywords: *Soil amendments; Biochar; Soil moisture retention; Seed germination; Ear length; Hyper-arid zones.*

1. INTRODUCTION

The agricultural sector is crucial for Algeria's economic diversification, contributing over 13% to the national GDP and employing 10% of the workforce. Driven by a surging consumption rate of 115 kg/capita/year, potato cultivation in El Oued city expanded from 628 hectares in 1999 to over 40,000 hectares by 2022. However, this boom relies on highly permeable quartz sand matrices, making crop survival entirely dependent upon extracting non-renewable groundwater from fossil aquifers via center-pivot irrigation. This hyper-arid nexus is severely constrained by intense solar radiation, which drives extreme soil surface temperatures and massive evaporative

demands, with over 80% of local farmers explicitly reporting rising ambient temperatures. Consequently, introducing local carbonaceous matrices like biochar emerges as a vital eco-geographic adaptation strategy to cushion the soil microenvironment against this solar-driven loading, decoupling crop productivity from unsustainable water expenditures [1-3].

From a development economics perspective, regional diagnostics across 75 local farms reveal that potato cultivation is heavily constrained by "unreasonable irrigation" protocols, short-term land renting that disincentivizes long-term soil management, and a rigid reliance on the 'Spunta' variety (two-thirds of production) which possesses a low dry matter content of 17%. This creates a profound spatial productivity gap that threatens structural development failures relative to national growth visions. Transforming regional agro-waste into biochar serves as a form of localized green industrialization, closing this spatial productivity gap by structurally re-engineering Saharan sand to optimize moisture retention and stabilize fragile root zones against severe solar desiccation [4,5].

At the micro-architectural scale, a 2% corn stalk biochar application significantly alters soil properties, boosting microbial respiration across aggregates during the initial 35 days—particularly within macroaggregates (2000-250 μm)—while enhancing the stability of microbial co-occurrence networks [6]. Beyond microbial shifts, biochar actively primes the intrinsic biological defense mechanisms of soil fauna. Pre-exposing ants (Formica japonica) to biochar-enriched substrates prior to heavy metal exposure improves survival rates from 60.3% to 83.0% and reduces cadmium (Cd) and lead (Pb) bioaccumulation by over 32% via transcriptomic path coordination [7]. Furthermore, a 5% biochar amendment interacts with soil organic components to reduce pesticide bioavailability (glyphosate, imidacloprid, and pyraclostrobin) by over 61%, shortening their half-lives by modifying root exudates and upregulating plant metabolic pathways [8].

The remediation efficiency of biochar relies on an intricate adsorption-desorption nexus. A 5% application rate of agro-waste biochars (banana peel, orange peel, or peanut husk) optimizes surface functional groups for maximum lead (Pb) and chromium (Cr) adsorption after 60 days, while keeping desorption rates low [9]. On a global scale, a meta-analysis of 1,143 paired observations shows that moderate biochar applications (10-30 t ha^{-1}) mitigate climate impacts by reducing methane (CH_4) by 18.11% and nitrous oxide (N_2O) by 15.54%, lowering overall global warming potential (GWP) by 25.51% while increasing total soil carbon stocks by 69.96% and crop yields by 11.13% [10]. However, these geochemical dynamics are highly temporal; in flooded, arsenic-contaminated environments, biochar triggers a stage-dependent counteracting effect, temporarily mobilizing arsenic via reductive dissolution during the first 14 days before shifting to organo-mineral immobilization by day 30 [11].

Despite temporal variations, biochar systematically mitigates severe abiotic stress in degraded profiles. In aluminum (Al^{3+})-enriched systems, tea-waste biochar regulates soil pH, lowers exchangeable aluminum levels, and improves ionic homeostasis while activating antioxidant metabolism to prevent cellular oxidative damage in seedlings [12]. Long-term hydrology monitoring also proves its value; a single 32.5 t ha^{-1} application of Populus nigra biochar over two years reduces runoff volume by 20% and soil loss by 24% by enhancing soil porosity and aggregate stability [13]. In nutrient-deficient subtropical forest soils, biochar counters the negative impacts of litter removal by stimulating acid phosphatase activity and increasing labile inorganic phosphorus (P) availability [14]. Similarly, in highly weathered Amazon Ferralsols, a 40 t ha^{-1} biochar application offers an affordable alternative to liming, reducing exchangeable Al^{3+} by up to 53%, increasing pH by 0.52 units, and enhancing plant potassium (K) accumulation by 55% [15].

Decadal field data confirms the long-term persistence of these effects. Twelve years after a single application (10-30 t ha^{-1}), biochar continues to maintain elevated extractable organic carbon and nitrogen pools, permanently restructuring microbial community networks [16]. Finally, biochar's efficiency varies based on baseline soil properties and water management. While it increases macro-nutrient bioavailability by 11–127% across varying soils, it mitigates heavy metal accumulation (by 11–80%) and microplastic stress effectively in acidic environments, but shows limited efficacy or even increases target metal uptake in alkaline profiles [17]. When integrated with alternate wetting and drying (AWD) irrigation, 20 t ha^{-1} of maize straw biochar reduces water percolation by 9% and dissolved P leaching by 20%, partitioning available P within the 0–40 cm layer while inhibiting its deep migration into the subsoil profile by over 119% [18]. Furthermore, the fundamental hydro-

thermal affinity between carbonaceous matrices and water molecules has been observed to extend into solar thermal applications; previous work utilizing natural charcoal blocks as porous absorbers demonstrated an 8% improvement in solar still freshwater productivity due to enhanced capillary action and optimized heat transfer dynamics [19].

While these diverse studies from current literature establish the extensive chemical, microbial, and macro-scale hydrologic benefits of biochar, there remains a critical knowledge gap regarding how escalating micro-dosage rates directly govern the hourly, diurnal thermo-physical properties of desert sands during early crop establishment. Therefore, this study utilizes a controlled 5-pot experimental matrix using aeolian Saharan sand to investigate the hourly dynamics of soil moisture desorption, pot temperature variations under direct solar exposure, and the subsequent early morphological growth performance of wheat (Triticum aestivum L.) seedlings.

2. MATERIALS AND METHODS

2.1. Experimental Site and Environmental Conditions

The field experiment was conducted at the experimental farm of the University of El Oued, located in southeastern Algeria. This region is characterized by an arid Saharan climate with high thermal amplitudes, low erratic rainfall, and a predominantly sandy soil profile (Saharan dunes sand) featuring high macro-porosity and poor natural water-holding capacity. Situated in southeastern Algeria, the El Oued region spans a total land area of approximately 54,573 km^2 and supports a population of nearly 700,000 residents. Geographically, the area is positioned at decimal coordinates 33.3683° N latitude and 6.8674°E longitude, sitting at a mean elevation of 60 m above sea level [20].

2.2. Materials and Soil Amendments

The experimental framework utilized a baseline soil matrix consisting of native, uncultivated Saharan sand collected locally from the El Oued region. Microscopic characterization of the sand matrix (as shown in Figure 1) reveals a distinct bimodal grain size distribution consisting primarily of fine and medium sand fractions. Optical analysis indicates that the grain boundaries consist predominantly of sub-rounded to angular structures characterized by two dominant particle diameter (d_p) configurations: a dominant fine fraction at d_p = 143.32µm and a secondary larger fraction at d_p = 292.96 µm, varying locally across sampled fields in distribution ratios ranging from 73.69% to 81% for the fine grains, and 19% to 26.31% for the larger grains.

To amend this sandy matrix, three distinct treatments were introduced:

- **Biochar:** The biochar utilized was a highly porous carbonaceous material produced via slow pyrolysis of local plant biomass under controlled high-temperature conditions (>350°C) in the complete absence (0%) of oxygen (O_2), adhering to standard processing guidelines (Lehmann and Joseph, 2009).
- **Organic Matter (OM):** A locally prepared composted organic matrix, integrated to stabilize structural aggregates and enrich baseline carbon levels.
- **Nitrogen (N):** A standard synthetic mineral nitrogen fertilizer, incorporated to evaluate potential chemical-nutrient synergies and plant uptake kinetics within the amended Saharan sand.

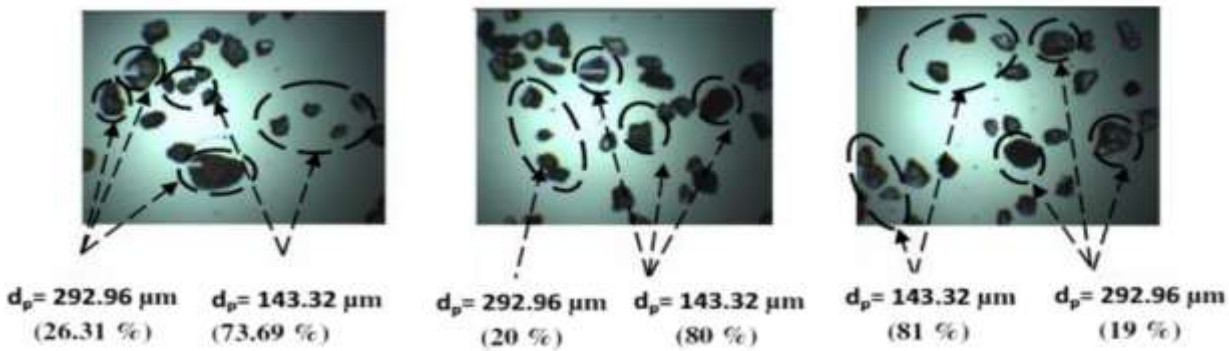

Figure 1. Microscopic analysis of the native Saharan sand matrix illustrating particle diameter (d_p) distribution and grain morphology [21]

2.2.1 Artisan Biochar Production Protocol

To transform raw agricultural waste into a stabilized soil amendment using a localized, low-cost artisan approach, a sequential five-stage thermochemical process was implemented, as illustrated in **Figure 2**:

1. **Stage 1: Raw Biomass Sourcing and Preparation:** Local, dry agricultural plant residues were gathered from surrounding agricultural fields. These residues were thoroughly air-dried under natural desert conditions to eliminate baseline moisture content prior to thermal processing, ensuring optimal energy efficiency during conversion.
2. **Stage 2: Open Ignition and Combustion Phase:** The dry plant biomass was initially ignited in an open-air environment to establish an active combustion front. This rapid heating phase triggers the primary structural breakdown of the lignin and cellulose materials, quickly elevating the core temperature required for subsequent carbonization.
3. **Stage 3: Oxygen Isolation and Pyrolysis Execution:** To transition the exothermic reaction from open combustion to slow pyrolysis, the burning biomass was rapidly isolated from ambient atmospheric oxygen. This was achieved using a physical barrier consisting of a sealed metal kiln buried within local soil to prevent air leakage. This oxygen-deprived, high-heat environment forced the organic matter to undergo destructive distillation, successfully driving off volatile gasses through a single localized exhaust vent while converting the solid fraction into high-purity carbonized matter rather than mineral ash.
4. **Stage 4: Thermal Stabilization and Recovery:** Following the complete consumption of volatile fractions, the sealed system was allowed to cool under completely airtight conditions to prevent secondary ash combustion. The recovered stabilized biochar exhibited a highly stable, aromatic carbon skeleton characterized by elevated micro-porosity and an expansive specific surface area.
5. **Stage 5: Substrate Integration and Plot Application:** In the final phase of the preparation protocol, the stable biochar was mechanically crushed into uniform, fine particles. This carbonaceous material was then thoroughly integrated into the native aeolian desert sand matrix at specific weight percentages across the designated experimental treatment plots to evaluate its long-term impacts on subsurface thermal dynamics, moisture retention, and seedling vegetative performance.

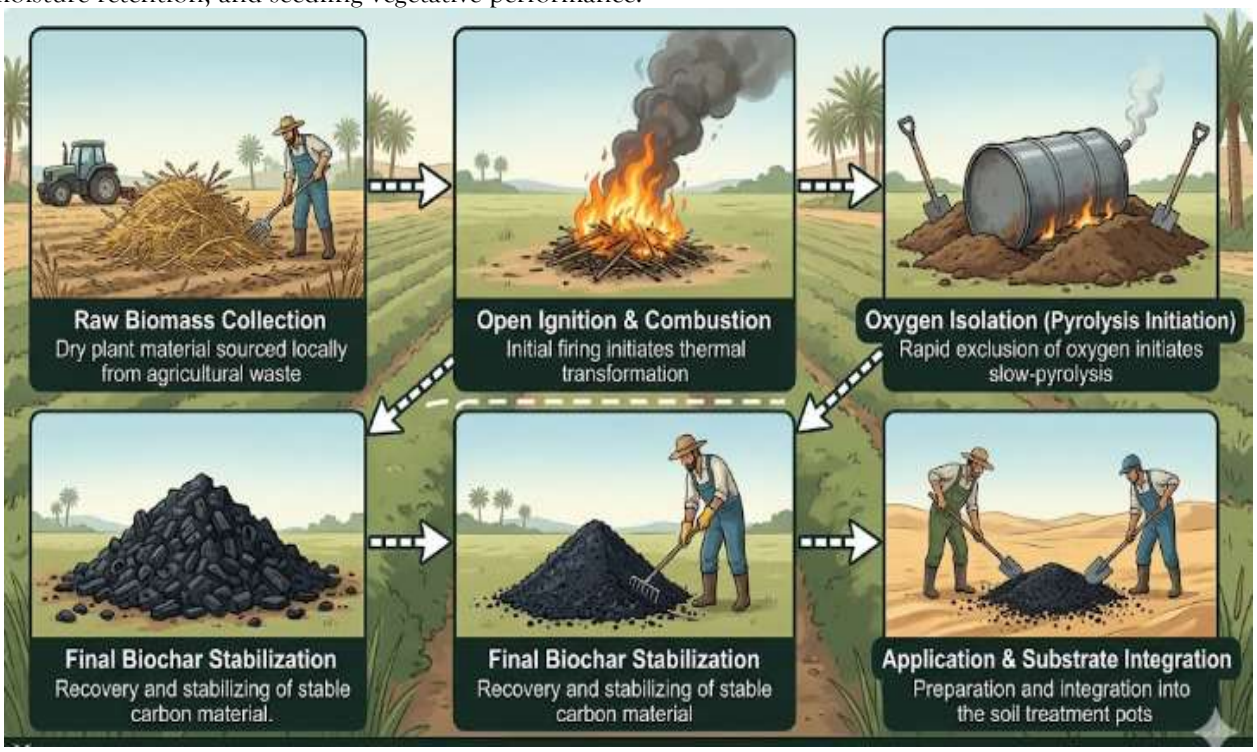

Figure 2. Schematic flowchart outlining the five sequential stages of artisan biochar production, processing, and soil matrix integration.

2.3. Experimental Design and Treatment Layout

The field experiment was arranged in a completely randomized design (CRD) with three independent replications for each treatment, resulting in a total of 24 experimental plots.

To systematically isolate the individual and synergistic effects of the amendments on the coarse sand matrix, eight distinct treatment formulations (To through T7) were established. The specific composition and structural breakdown of each evaluated plot matrix are detailed in Table 1.

Table 1. Detailed composition and amendment breakdown of the eight experimental treatments

Treatment Code	Matrix Description & Composition Breakdown	Target Application Purpose
T0	Pure Native Saharan Sand (0% Amendments)	Absolute Control Baseline
T1	Sand + Composted Organic Matter (OM)	Binary Organic Control
T2	Sand + Low-Dose Mineral Nitrogen (N)	Nutrient Control Baseline
T3	Sand + Pure Artisan Biochar	Binary Carbonaceous Matrix
T4	Sand + Biochar + Organic Matter (OM)	Ternary Physicochemical Blend
T5	Sand + Biochar + Mineral Nitrogen (N)	Carbon-Nutrient Synergy Blend
T6	Sand + Biochar + Organic Matter (OM) + Nitrogen (N)	Fully Optimized Composite Matrix
T7	Sand + Organic Matter (OM) + Nitrogen (N)	Non-Char Organic-Nutrient Control

All amendments were thoroughly incorporated into the top 20 cm layer of the designated sand plots to mimic a realistic crop root-zone profile. Following matrix stabilization, uniform wheat seeds were sowed across all 24 plots under identical baseline conditions to initiate the monitoring cycle.

2.4. Laboratory Protocols and Hydrodynamic Characterization

To contextualize the macro-physical behaviors observed in the field, targeted laboratory characterization tests were executed to isolate and evaluate biological and physical matrix behaviors.

2.4.1 In Vitro Matrix Incubation Assay

To evaluate the biological baseline of the modified matrices on organic matter decomposition kinetics, a standardized *in vitro* laboratory incubation assay was performed in triplicate (n = 3) as shown in Figure 3. A total of 21 Petri dishes were organized across seven comparative structural baselines: pure sand (To), pure organic matter (OM_{pure}), pure biochar (BC_{pure}), ternary mixture (T4), and binary control formulations (T1, T3, and BC+ OM).

Each experimental unit received a uniform, standardized dry matrix layer. Uniformly sized fragments of fresh vine leaves 1cn x 1 cm) were introduced into each Petri dish to serve as the baseline organic decomposition substrate. Following hydration with 10 mL of distilled water, the entire experimental matrix was subsequently transferred into a controlled incubator maintained in complete darkness to isolate microbial metabolic action from photosynthetic or light-induced interference.

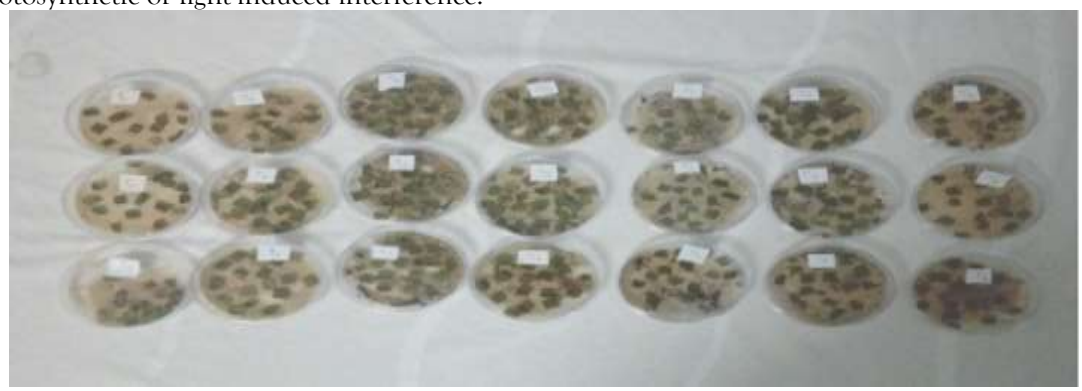

Figure 3. Experimental layout of the in vitro microbiological matrix incubation assay.

2.4.2 Physical Water Infiltration and Hydrodynamics

On January 27, 2018, a hydrodynamic filtration test was carried out to quantify how the matrix structural modifications alter the soil's hydraulic conductivities and percolation behavior as shown in Figure 3. The assessment evaluated water retention capacity and infiltration dynamics across the primary modified configurations: pure sand (To), sand supplemented with biochar and organic matter (T4), sand with biochar (T3), and sand with organic matter (T1).

Infiltration capacity was determined by recording the precise temporal duration (expressed in seconds, s required for a constant volume of 1.5 L of distilled water to completely filter through identical volumetric columns of each prepared substrate under gravity-fed conditionsm as shown in Figure 4.

Figure 4. Filtration test

2.5 Field Monitoring and Agronomic Quantifications

2.5.1 Subsurface Moisture and Thermal Tracking

Following the field installation, physical soil parameters were systematically tracked over a continuous 16-day monitoring cycle. Volumetric soil moisture content (%) was recorded daily across all 24 experimental plots (comprising all eight treatment modalities, T0 to T7, in triplicate) to evaluate the hydro-retentive efficacy and desiccation speed of each amendment formula under the high evaporative demands of the Saharan climate.

Concurrently, a network of electronic temperature sensors was strategically embedded within the root-zone profile of the plots to capture continuous diurnal thermal cycles and vertical soil temperature gradients. Scheduled, documented irrigation events were initiated dynamically whenever soil moisture levels neared critical depletion thresholds to analyze the subsequent moisture recovery kinetics and matrix recharge capacity of the treated soils.

2.5.2 Agronomic Performance Indicators (Germination & Yield)

To explicitly link soil hydrodynamic performance with biological productivity and resolve the relationship between early establishment and final crop output, plant vital signs were quantified across two critical phases:

1. Seed Germination Percentage (%): The final seedling emergence rate was quantified across all eight treatment modalities (T0–T7) at the conclusion of the early vegetative seedling establishment phase. This metric was determined by calculating the precise ratio of successfully emerged coleoptiles to the total number of sowed seeds within each experimental plot.
2. Final Plant Performance (Ear Length): At the conclusion of the crop's vegetative and reproductive life cycle, final agronomic productivity was evaluated at maturity. Representative crop samples were harvested from each treatment group to measure the average ear length (expressed in centimeters, cm), providing the final quantitative dataset required to evaluate long-term amendment efficacy.

3. RESULTS AND DISCUSSION

The microclimatic variables, specifically solar radiation and ambient air temperature, represent the primary environmental drivers regulating sub-surface thermal behavior, evaporation rates, and the overall physiological demands of the crop.

Figure 5 presents the chronological evolution of the average diurnal profiles for solar radiation W/m^2 and ambient air temperature (°C) recorded during the experimental monitoring period in February. The meteorological data exhibited typical diurnal fluctuations characteristic of the hyper-arid Saharan climate of El Oued city, Algeria. The solar radiation intensity reached its diurnal peak during midday hours, maximizing at approximately 700 W/m^2 which directly drove the thermal loading on the soil surface. Concurrently, the ambient air temperature lagged slightly behind the solar peak, fluctuating between a nocturnal minimum of 7.5°C at dawn and a mid-afternoon maximum of 20.5 °C.

These ambient climatic conditions imposed a high atmospheric evaporative demand, thereby directly influencing the sub-surface soil moisture dynamics, driving thermal stress in unamended matrices, and shaping the early vegetative development stages of the plants.

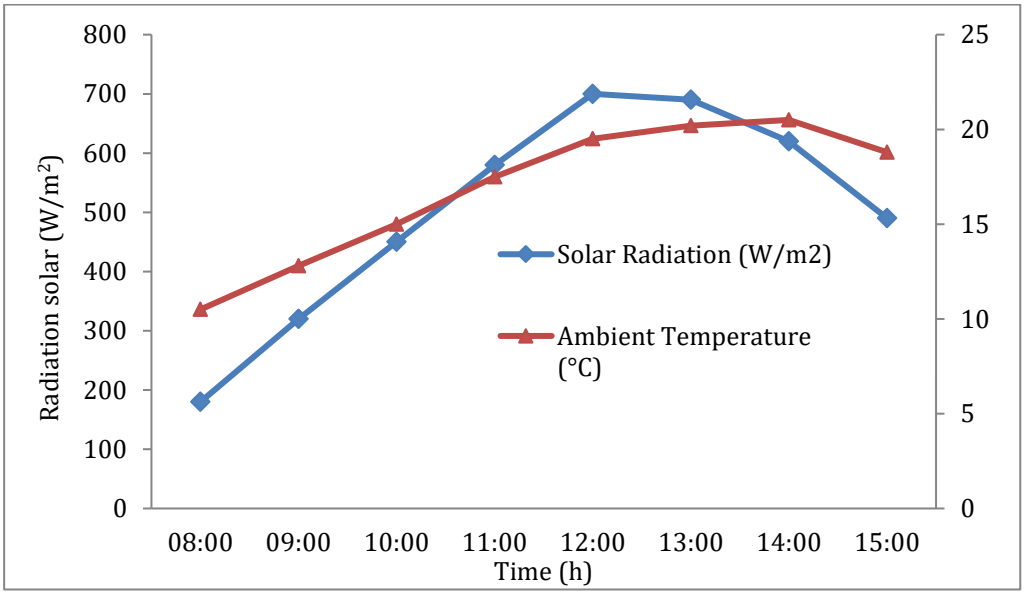

Figure 5. Diurnal evolution of average solar radiation intensity and ambient air temperature during the February experimental period in the hyper-arid environment of (El Oued, Algeria).

3.2.1 Analysis of Maximum and Minimum Moisture Values

The hydrodynamic performance of the monitored plots revealed distinct structural turning points during the continuous 16-day tracking period:

- Maximum Moisture Content (Day 1): The absolute highest moisture values were achieved immediately following the initial saturation phase on Day 1. The carbonaceous biochar-amended plots, specifically T3 (Pure Biochar) and T4 (Biochar + Organic Matter), attained peak moisture saturation levels of 100%, followed closely by the complex structural composite T6 (98%). In contrast, the unamended control sand (T0) reached a maximum of only 80% water content, demonstrating an immediate physical restriction in initial water absorption volume due to its poor capillary network.
- Minimum Moisture Content and Desiccation Kinetics: The absolute lowest moisture levels during the primary drying cycle were recorded between Day 5 and Day 8. The native desert sand (T0) exhibited an aggressive, rapid moisture collapse, plunging to a critical absolute minimum of 0% by Day 5 and remaining completely desiccated until Day 8. This total desiccation point represents a complete depletion of plant-available water. While treatment T1 also dropped to 0% by Day 7, the biochar treatments (T3, T4) successfully resisted this severe drop, maintaining an elevated moisture buffer of 70% on Day 5 and dropping no lower than 30% during their maximum drying phase on Day 9 before targeted re-irrigation events stabilized the matrix.

3.2.2 Comparative Treatment Performance and the Impact of Biochar

The experimental data across the full 16-day period clearly demonstrates (Figure 6) that the introduction of biochar significantly enhanced the soil's hydro-retentive capacity compared to all other configurations:

- The Hydrodynamic Collapse of Native Sand (T0, T1, T2): Due to the high macro-porosity, minimal specific surface area, and lack of cohesive matrix suction inherent to raw Saharan quartz sand, the unamended control (T0) was fundamentally incapable of holding water against gravity drainage and intense surface evaporation. This forced a pattern of rapid moisture crashes followed by mandatory, frequent re-irrigation interventions (visible via the artificial moisture spikes on Day 9, Day 12, and Day 15/16).
- The Biochar Water Reservoir (T3, T4, T5, T6): Biochar treatments radically altered this behavior, maintaining stable moisture levels above 60% deep into the cycle and effectively extending irrigation intervals. The high porosity and immense specific surface area of biochar particles act as a microscopic sponge within the sandy matrix. This increases the volume of narrow capillary pores, holding water tightly against gravity while significantly retarding vertical vapor transport.
-

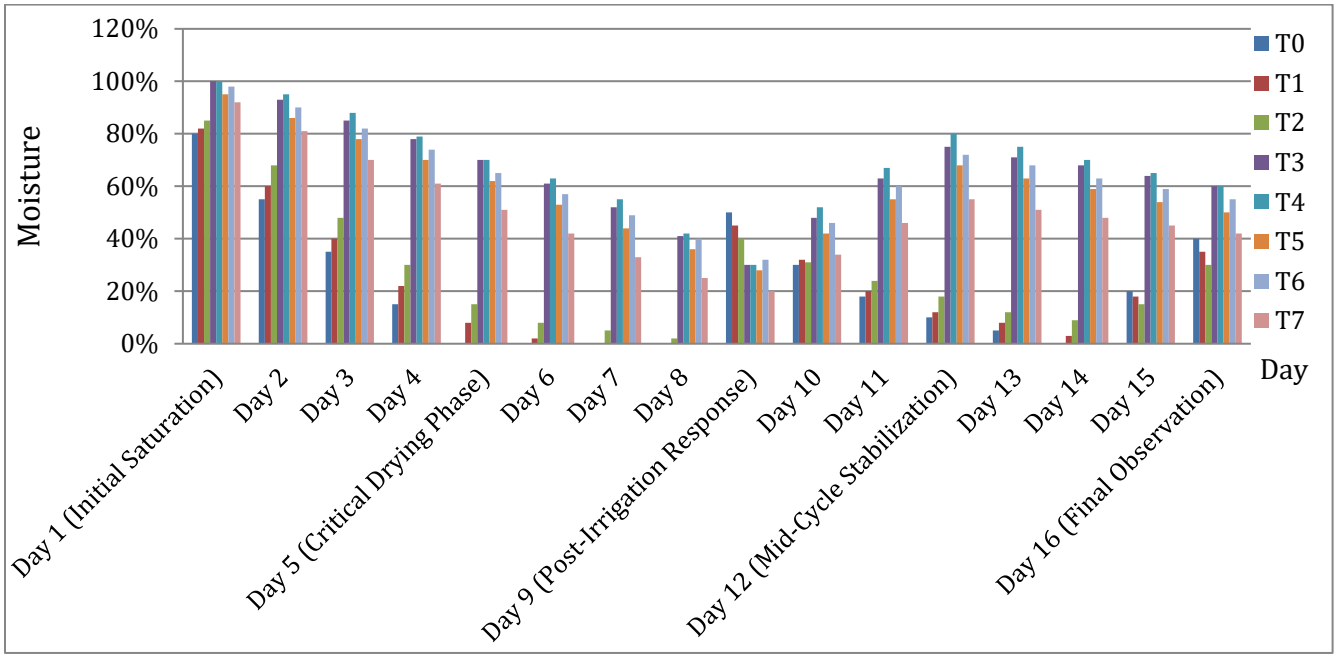

Figure 6. Dynamic profiles of soil moisture.

3.3 Effect of Soil Amendments on Seed Germination

The initial establishment phase of a crop is highly sensitive to the physical and chemical microenvironment of the surrounding soil matrix. To evaluate the early biological response to the modified Saharan sand, the final seed germination percentage was recorded across all experimental modalities T0 to T7).

As visually outlined in Figure 8, the final seed germination percentage exhibited a distinct, descending trend across the evaluated soil configurations, moving from the unamended controls toward the more structurally complex matrices.

- The High-Velocity Emergence in Native Sand (T0): The unamended control sand reached the absolute highest final germination rate at 93%. Raw desert sand acts as a highly macro-porous, loose, and uninhibited physical medium. Because there are no binding agents or heavy organic elements to physically block the seedlings, the coleoptiles encountered minimal mechanical resistance, allowing for rapid and widespread initial emergence.
- The Performance of Biochar Mixes (T4 and T3): The plots containing carbonaceous biochar performed very well, with the biochar-organic matter blend (T4) achieving 90% and pure biochar (T3) reaching 89%. These high rates prove that while biochar modifies the bulk density of the soil, it maintains excellent aeration and aeration-to-moisture ratios that support healthy seed activation.
- The Critical Germination Suppression in T2: Conversely, treatment T2 suffered from severe early-stage limitations, dropping to the absolute lowest germination success rate of just 50%. This heavy suppression

indicates potential mechanical impedance or localized osmotic imbalances in the seed zone, which severely blocked early radical penetration.

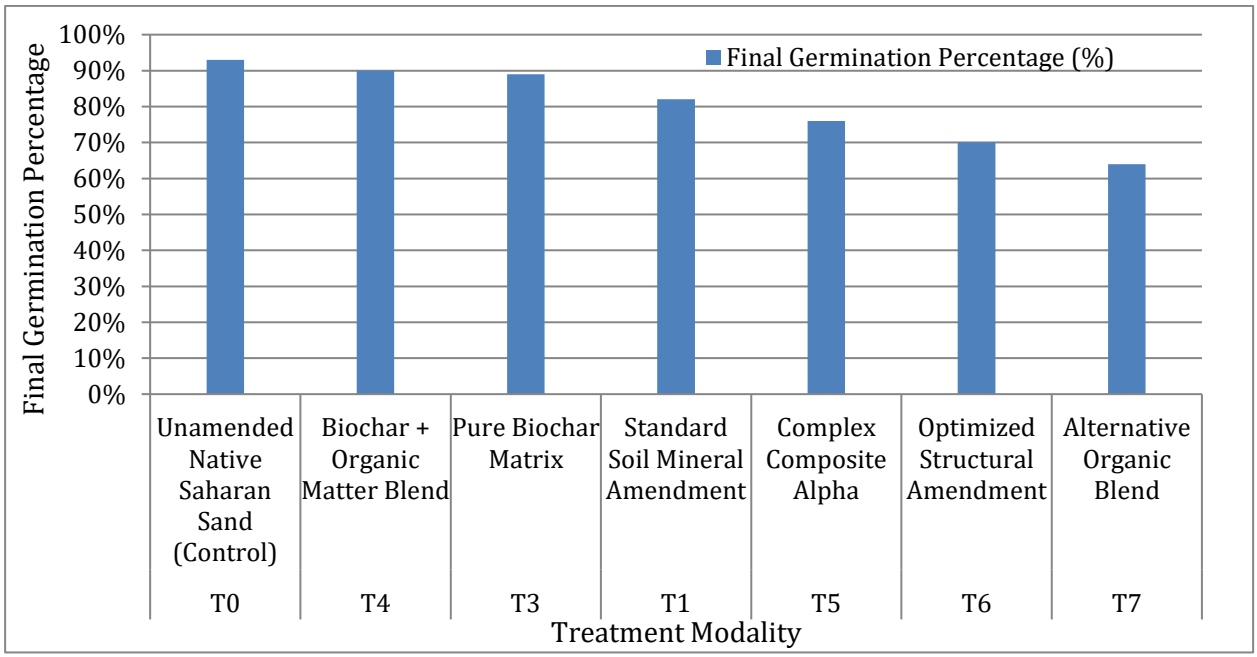

Figure 8. Comparative breakdown of final seed germination percentages (%) showing the immediate physical response of the crop to different soil conditions.

3.4 Effect of Treatments on Final Plant Performance

To evaluate the ultimate structural efficacy and practical field value of the applied soil adjustments, the final agronomic yield was quantified via comprehensive ear length measurements at the conclusion of the crop's vegetative and reproductive life cycle. The comparative data points detailing the ultimate performance across all experimental cohorts are systematically organized in Figure 9 and Table 4.

Table 4. Final agronomic crop performance evaluated via comparative ear length (cm).

Treatment Modality	Description of Matrix Amendment	Final Average Ear Length (cm)
T6	Optimized Structural Amendment	**18.0 (Absolute Maximum)**
T5	Complex Composite Alpha	17.0
T3	Pure Biochar Matrix	16.0
T4	Biochar + Organic Matter Blend	16.0
T1	Standard Soil Mineral Amendment	14.5
T7	Alternative Organic Blend	13.0
T0	Unamended Native Saharan Sand (Control)	**12.0 (Heavily Stunted)**
T2	Low-Dose Structural Conditioner	11.5

The structural yield data collected at harvest revealed a complete (Figure 4), systematic inversion of the initial trends recorded during the seedling emergence phase:

- The Dominance of Advanced Modifications (T6, T5): The longest ear lengths were successfully achieved under treatment T6, reaching an impressive 18.0 cm, followed closely by T5 at 17.0 cm. Furthermore, both biochar-centric cohorts (T3 and T4 displayed robust, highly reliable structural outputs, capping stably at 16.0 cm.
- The Failure of the Control Matrix (T0): In stark contrast to its early performance, the unamended control sand (T5) finished as one of the poorest performing groups, producing heavily stunted ears that capped at a meager

12.0 cm. The only group that scored lower was T2 (11.5 cm), which never recovered from its poor 50% germination baseline.

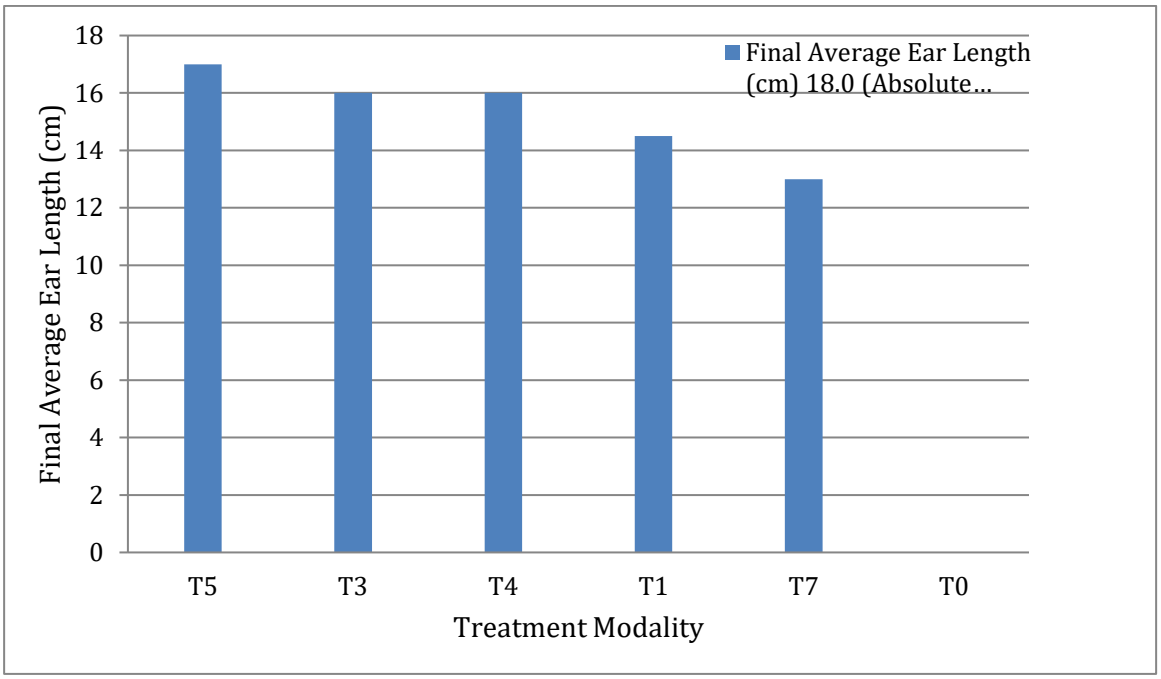

Figure 9. Final plant yield comparison based on average ear length (cm) highlighting the long-term benefits of structural soil modifications.

4. DISCUSSION

4.1. Hydro-Thermal Dynamics and Pore Restructuring

The hyper-arid climatic conditions of El Oued, characterized by intense midday solar radiation (~700 W/m^2), drove the rapid moisture collapse observed in the unamended sand (T0). Because raw Saharan quartz sand is dominated by large macro-pores with negligible matrix suction, it cannot retain water against gravity drainage and solar evaporation.

Integrating fine artisan biochar particles fixes this structural flaw. The highly porous internal skeleton and immense specific surface area of the biochar particles allow them to lodge within the inter-granular sand voids, creating a dense network of capillary micro-pores. This capillary network exerts strong matrix suction forces that lock water molecules in place and retard vertical vapor escape, successfully maintaining the 70% moisture buffer deep into the drying cycle.

4.2. The Germination-to-Yield Paradox

A key finding is the complete inversion of performance trends between initial seedling emergence and final harvest. The loose, macro-porous structure of pure sand (To) initially offered zero physical resistance to emerging coleoptiles, allowing a high 93% germination rate. However, without a structural amendment, these plants suffered extreme water and nutrient starvation during maturity under the desert sun, resulting in heavily stunted ears (12.0 cm).

Conversely, complex treatments like T6 and T5 achieved the absolute maximum ear lengths (18.0 cm and 17.0 cm, respectively). While the dense amendments caused minor mechanical impedance at germination, they paid massive physiological dividends over time. The prolonged root-zone moisture reservoir and steady nutrient availability provided a stress-free microenvironment during critical reproductive phases, optimizing grain fill.

4.3. Carbon-Water Interface Mechanisms

The microscopic processes governing water retention in these biochar-amended sands mirror the physical mechanisms found in solar desalination systems. In single-slope solar distillers, inserting natural, pyrolyzed carbon blocks into the basin enhances capillary water drawing and heat transfer, driving an 8% increase in cumulative freshwater distillation yield.

When distributed within aeolian sand, these same porous carbon architectures utilize their inherent capillary action to regulate water pathways. Instead of allowing rapid upward vaporization into the atmosphere, the biochar's capillary matrix anchors the moisture within the crop root-zone, converting an open evaporative loss into a productive, plant-available subsurface water reservoir.

5. CONCLUSION

This study systematically investigated the structural and biological efficacy of integrating diverse soil amendments (T0 to T7) within the coarse, hyper-arid sandy matrices of the Souf Valley, Algeria. Based on the rigorous 16-day hydrodynamic tracking and agronomic performance assessments, the following definitive conclusions can be drawn:

- Microclimatic Evaporative Drivers: Core daytime meteorological tracking established a high-evaporative boundary layer, with solar radiation intensity shifting from 180 W/m^2 to a noon peak of 700 W/m^2, driving an ambient thermal trajectory that maximized at 20.5 °C . This intense atmospheric demand catalyzed rapid subsurface desiccation in unamended fields.
- Hydrodynamic Buffering capacity: Structural amendments fundamentally reshaped soil hydraulic traits. Native desert sand (T0) failed to maintain plant-available water against surface evaporation and gravity drainage, experiencing a total moisture collapse to 0% by Day 5. In contrast, pure biochar (T3) and biochar-organic matter blends (T4) acted as an internal microscopic sponge, absorbing maximum initial saturation volumes (100%) and maintaining an active water-holding buffer (70%) deep into the drying cycle.
- Validation of the Agronomic Paradox: The investigation successfully verified a vital agronomic paradox. Raw quartz sand (T0) provided a loose, uninhibited physical medium that minimized physical impedance for sprouting coleoptiles, achieving the maximum initial germination success of 93%. However, this early vegetative head start was thoroughly neutralized during reproductive stages due to the matrix's poor retentive properties.
- Final Yield Maximization: Ultimate crop productivity trends completely inverted the initial germination behaviors. The untreated control sand (T0) concluded the lifecycle with heavily stunted ears measuring just 12.0 cm. Conversely, the optimized complex amendment T6 successfully supported the plant through critical reproductive windows, yielding the absolute longest average ear length at 18.0 cm, followed closely by T5 (17.0 cm) and the biochar cohorts (16.0 cm).

In summary, successful seedling emergence alone does not guarantee superior final crop yields in desert farming. For sustainable agriculture in hyper-arid regions like El Oued, the deployment of structured amendments particularly optimized composite matrices (T6) and carbonaceous biochar blends is highly recommended to secure the permanent hydro-thermal and nutritional buffering required to transform raw sand into highly productive, resilient cultivation mediums.

REFERENCES

1. Sais, H. A., Merrouchi, L., Fethallah, R., & Fahas, M. (2026). Dynamics of potato cultivation in the arid Saharan region of El Oued (Algeria) and farmers' perceptions and adaptations to climate change. Annals of Arid Zone, 65(1), 209–219. https://doi.org/10.56093/aaz.v65i1.173200

2. Djouhri, N., Bouammar, B., & Dadamoussa, M. L. (2023). Study of the sustainability of potato farms in the region of Oued Souf (Southern Algeria). Turkish Journal of Agriculture - Food Science and Technology, 11(2), 197–201. https://doi.org/10.24925/turjaf.v11i2.197-201.4861

3. Khechekhouche, A., Manokar, A. M., Sathyamurthy, R., Essa, F. A., Sadeghzadeh, M., & Issakhov, A. (2021). Energy, exergy analysis, and optimizations of collector cover thickness of a solar still in El Oued climate, Algeria. International Journal of Photoenergy, 2021, 6668325. https://doi.org/10.1155/2021/6668325

4. Meijer, B. J. M., Aissat, A., & Benchaalal, K. (2019). Potato storage and processing in Algeria; Study on potato processing and post-harvest chain in Algeria. Ministry of Agriculture, Nature and Food Quality of the Netherlands & Maastricht School of Management (MSM), 47 pp.

5. Mostefaoui, O., Mostefaoui, A., & Hemici, K. (2026). Geography of the digital paradox: A development economics perspective on Algeria's structural transformation (1994–2022). International Journal of Computational and Experimental Science and Engineering (IJCESEN), 12(2), 72–78. http://www.ijcesen.com

6. Zhang, D., Li, J., Zhang, Z., Wu, X., & Cheng, X. (2026). Divergent response of microbial traits in soil aggregates to biochar addition in degraded grassland of southwest China. Soil and Tillage Research, 262, 107241. https://doi.org/10.1016/j.still.2026.107241

7. Liu, S., Zeng, L., Xiong, D., Wu, M., Oleszczuk, P., Steinberg, C. E. W., Pan, B., Tao, S., & Xing, B. (2026). Enhanced resistance of ants (Formica japonica) reared on biochar-enriched soil to stress induced by heavy metals: Programming of the molecular defense system. Ecotoxicology and Environmental Safety, 319, 120326. https://doi.org/10.1016/j.ecoenv.2026.120326

8. Shi, G., Cao, X., Fu, Q., Li, T., Chen, Q., & Hou, R. (2026). Biochar and organic fertilizer reduce pesticide uptake in soybean via soil microbial community and root metabolic modifications. Soil and Tillage Research, 262, 107239. https://doi.org/10.1016/j.still.2026.107239

9. Nawab, J., Ruby, Hamza, A., Waqas, M., Magazzino, C., Kleinke, M., & Ullah, I. (2026). Adsorption-desorption nexus of biowaste-derived biochars towards potentially toxic elements: Unveiling challenges and paving paths for the large-scale mining and industrial soil applications. Biomass and Bioenergy, 213, 109371. https://doi.org/10.1016/j.biombioe.2026.109371

10. Sinha, A., Parihar, C. M., Panneerselvam, P., Sarkar, A., Reddy, K. S., Patra, K., Bharadwaj, S., Patra, M., Sharma, D. K., Jat, S. L., Rathore, S. S., Kumar, S., Sherpa, S. R., Nayak, H. S., & Kumar, V. (2026). Optimizing biochar use in rice production for improving soil health and environmental sustainability: A global meta-analysis guided insights. Soil Advances, 5, 100120. https://doi.org/10.1016/j.soilad.2026.100120

11. Fan, J., Liao, M., Duan, T., Fan, T., Sun, J., & Huang, B. (2026). Stage-dependent counteracting effects of biochar on arsenic mobilization and immobilization in paddy soil. Journal of Hazardous Materials, 512, 142373. https://doi.org/10.1016/j.jhazmat.2026.142373

12. Borah, S. P., Fernandes, S. R., Bhattacharjee, C. R., Ghosh, N. N., Kumar, S., Gupta, A., Ranjan, R. K., Das, S., & Choudhury, S. (2026). Biochar derived from tea processing waste residue improves the performance of tea seedlings growing in aluminium (Al^{3+}) enriched soil: A comprehensive analysis of stress responses and metabolic flux. Bioresource Technology, 455, 134861. https://doi.org/10.1016/j.biortech.2026.134861

13. Moafi, G., Gholami, L., Kavian, A., & Kheirfam, H. (2026). Two-year monitoring of biochar effects on soil and water conservation in USLE plots under field conditions. International Soil and Water Conservation Research, 100665. https://doi.org/10.1016/j.iswcr.2026.100665

14. Li, J., Zhu, Y., Zhu, H., Turner, B. L., Ding, S., Shen, W., Tan, Y., Ma, J., Bai, K., Yang, Z., Duan, M., & Turner, B. L. (2026). Contrasting responses of soil phosphorus dynamics to bamboo litter removal and its biochar amendment in a subtropical forest. Pedosphere. https://doi.org/10.1016/j.pedsph.2026.05.010

15. Danielli, C. K. A. O., Florentino, A. L., Danielli, F. E., Sousa, H. M., Braga, A. R. O., John, V., Falcão, N. P. S., Lavres, J., & Marques-dos-Santos, C. S. C. (2026). Açaí biochar reduced soil acidity and enhanced potassium and micronutrient availability in Amazon Ferralsol under cowpea cultivation. Biomass and Bioenergy, 214, 109378. https://doi.org/10.1016/j.biombioe.2026.109378

16. Mao, X., Zhang, X., Li, F., Xu, C.-Y., & Zhou, X. (2026). Twelve-year biochar application alters soil labile organic carbon, nitrogen pools and microbial diversity in a subtropical forest. Forest Ecology and Management, 615, 123830. https://doi.org/10.1016/j.foreco.2026.123830

17. Meng, J., Yao, C., Diao, C., Jia, S., Li, Z., Xu, J., Xu, Y., Yang, D., Shan, S., & Chen, H. (2026). Contrasting responses of soil-microbial-plant systems to co-application of biochar and microplastics with/without additives in acidic versus slightly alkaline heavy metal-affected soils. Environmental Research, 303(Part 2), 124735. https://doi.org/10.1016/j.envres.2026.124735

18. Zhang, W., Chi, D., Chen, T., Zhu, H., Liu, G., Wilson, L. T., & Li, G. (2026). Biochar-mediated soil phosphorus leaching and distribution behaviors in AWD paddy fields of a Northeast China alluvial plain. Agricultural Water Management, 324, 110155. https://doi.org/10.1016/j.agwat.2026.110155

19. A. Sadoun, A. Khechekhouche, I. Kemerchou, M. Ghodbane, and B. Souyei, "Impact of natural charcoal blocks on the solar still output," Heritage and Sustainable Development, vol. 4, no. 1, pp. 61–66, 2022. https://doi.org/10.37868/hsd.v4i1.80

20. A. Khechekhouche, B. Ben Haoua, A. E. Kabeel, M. E. H. Attia, and W. M. El-Maghlany, "Improvement of Solar Distiller Productivity by a Black Metallic Plate of Zinc as a Thermal Storage Material," Journal of Testing and Evaluation, vol. 49, no. 2, pp. 967–976, 2021. https://doi.org/10.1520/JTE20190119

21. A. Khechekhouche, B. Benhaoua, M. Manokar, and G. Sathyamurthy, "Sand dunes effect on the productivity of a single slope solar distiller," Heat and Mass Transfer, vol. 56, no. 4, pp. 1117–1126, 2020. https://doi.org/10.1007/s00231-019-02786-9